# Ground-state muon transfer from deuterium to $^3$He and $^4$He

B. Gartner,* P. Ackerbauer, W. H. Breunlich, M. Cargnelli, P. Kammel,† R. King, B. Lauss,‡ J. Marton, W. Prymas, and J. Zmeskal
*Institute for Medium Energy Physics, Austrian Academy of Sciences, Boltzmanngasse 3, A-1090 Vienna, Austria*

C. Petitjean
*Paul Scherrer Institut, CH-5232 Villigen, Switzerland*

M. Augsburger,§ D. Chatellard, and J.-P. Egger
*Institut de Physique de l'Université, CH-2000 Neuchâtel, Switzerland*

T. von Egidy, F. J. Hartmann, A. Kosak, and M. Mühlbauer
*Physik-Department, Technische Universität München, D-85747 Garching, Germany*

F. Mulhauser, L. A. Schaller, L. Schellenberg, H. Schneuwly, Y.-A. Thalmann, S. Tresch, and A. Werthmüller
*Institut de Physique de l'Université, CH-1700 Fribourg, Switzerland*

(Received 2 August 1999; published 7 June 2000)

We have observed the deexcitation x-ray spectra of the exotic molecules $(d\mu^4\mathrm{He})^*$ and $(d\mu^3\mathrm{He})^*$ with good statistics and low background. From the time distributions of these x rays, we have directly determined the muon transfer rates from ground-state muonic deuterium atoms to helium nuclei. The obtained transfer rates in gaseous mixtures at ~30 K are $\lambda_{d^3\mathrm{He}}=(1.856\pm0.077)\times10^8\ \mathrm{s}^{-1}$ to $^3$He, and $\lambda_{d^4\mathrm{He}}=(10.50\pm0.21)\times10^8\ \mathrm{s}^{-1}$ to $^4$He. In liquid mixtures, we measured the muon transfer rates $\lambda_{d^3\mathrm{He}}=(2.77\pm0.73)\times10^8\ \mathrm{s}^{-1}$ and $\lambda_{d^4\mathrm{He}}=(14.2\pm1.4)\times10^8\ \mathrm{s}^{-1}$. These transfer rates have to be multiplied with the target density and the atomic helium concentration to obtain the ''effective transfer rates'' for a specific target composition. The expected isotopic effect between mixtures containing $^3$He and mixtures containing $^4$He, as well as with respect to the hydrogen-helium case, is clearly confirmed. A density effect was observed for both isotopic compositions. We investigated the widths and the energies of the intensity maxima of the observed energy spectra of the molecular x rays. From the comparison of the measured energy spectra with calculated ones, we conclude that decay from the rotational state $J=1$ of the muonic molecule dominates over decay from $J=0$ at the investigated experimental conditions.

PACS number(s): 36.10.Dr, 34.70.+e, 33.20.Rm, 82.30.Fi

## I. INTRODUCTION

### A. Muon transfer process

Muonic molecules are a valuable tool to test theoretical atomic and molecular models because many observables are larger than those in the analogous electronic system, due to the heavier mass of the muon. The muon transfer rate from hydrogen to helium is of particular interest in view of its connection to the classical case of muon catalyzed fusion ($\mu$CF), namely, the muon induced fusion of the nuclei of two hydrogen isotopes [1]. Muon transfer to helium is a muon loss channel for the fusion cycle, and $^3$He or $^4$He are continuously produced by the fusion process and accumulated in the target. Additionally, in mixtures containing tritium, the $^3$He content constantly increases due to nuclear $\beta$ decay of tritium.

Direct transfer of negative muons from the ground state of muonic hydrogen $(\mu h)_{1s}$ and its isotopes ($h$ stands for any hydrogen nucleus: proton $p$, deuteron $d$, or triton $t$, $\mu$ indicates the muon) to high-$Z$ nuclei (nuclei with charge $Z\geqslant3$) occurs with rates of the order of $10^{11}\ \mathrm{s}^{-1}$ [2]. The $h\mu$He system (He is the respective helium isotope $^3$He or $^4$He) is exceptional among the $h\mu Z$ systems. Long ago, it was pointed out for the equivalent electronic system that the molecular term $2p\sigma$, which corresponds to the separated hydrogen atom in the ground state, has a small attractive potential and does not cross the $1s\sigma$ term, which corresponds to the ground state of the helium ion $He^{2+}$ [3]. Calculations for the muonic system lead to small transfer rates of the order of $\sim10^6\ \mathrm{s}^{-1}$, which was explained analogously by the absence of crossings and pseudocrossings of these terms [4]. At the beginning of the 1980s, a muon exchange mechanism via the formation of an excited, metastable hydrogen-helium-molecule $(h\mu\mathrm{He})^*$ was proposed [5]. This mechanism predicted transfer rates up to two orders of magnitude higher than the direct transfer process.

The processes are described on the example of the deuterium-helium case here, since this paper is devoted to the measurements in deuterium-helium ($D_2$-He) mixtures. The muonic molecules are formed in collisions of ground-

*Electronic address: bettina@amuon.imep.univie.ac.at
†Present address: University of California and L. Berkeley National Laboratory, Berkeley, CA 94720.
‡Present address: Lab. Naz. di Frascati dell'INFN, I-00044 Frascati, Rome, Italy.
§Present address: Institut de Physique de l'Université, CH-1700 Fribourg, Switzerland.

 

state muonic hydrogen atoms with helium:

$$(\mu d)_{1s} + \mathrm{He} \rightarrow [(d\mu\mathrm{He})^* e^-]^+ + e^-. \quad (1)$$

The binding energy is carried off by an Auger electron. Muonic hydrogen-helium molecules only exist in the state $2p\sigma$ with the vibrational quantum number $\nu = 0$. All other molecular states are unbound. The resonant metastable molecular state deexcites to its unbound ground state $1s\sigma$. The released energy is carried off by the emission of an x ray of well-defined energy ($\sim$6.8 keV),

$$[(d\mu\mathrm{He})^* e^-]^+ \rightarrow [(d\mu\mathrm{He})^{2+} e^-]^+ + \gamma, \quad (2)$$

or by an Auger electron of the same energy:

$$[(d\mu\mathrm{He})^* e^-]^+ \rightarrow (d\mu\mathrm{He})^{2+} + e^-. \quad (3)$$

The probability of x-ray transition is significantly higher than that by emission of an Auger electron. The molecule dissociates to the nucleus of the hydrogen isotope and a muonic helium atom

$$(d\mu\mathrm{He})^{2+} \rightarrow (\mu\mathrm{He})^+ + d. \quad (4)$$

The energy difference between the $2p\sigma$ and $1s\sigma$ molecular states in the vicinity of the minimum of the $2p\sigma$ state is more than two orders of magnitude higher than in the analogous electronic system. After its proposal, the described muon transfer mechanism was studied theoretically in several publications [6–9]. The discussion was renewed with the suggestion of a possible nonradiative decay channel due to particle decay of the muonic molecule with the rate $\lambda_p$ [10]:

$$[(d\mu\mathrm{He})^*]^{2+} \rightarrow (\mu\mathrm{He})^+ + d + 8.2\ \mathrm{keV}. \quad (5)$$

The reaction products are accelerated by the released energy. $\lambda_p$ is sensitive to the rotational state of the muonic molecule and to its reduced mass, which generates a strong isotopic effect on the branching ratio of the decay channels: the probability of particle decay is three times higher for $(d\mu^3\mathrm{He})^*$ than for $(d\mu^4\mathrm{He})^*$. This is one of the reasons why x rays from radiative decay of the latter are easier to observe.

The shape of the emitted x-ray spectrum is asymmetric with an expected width of $\sim$0.8 keV. Most probably, a molecule is formed with a rotational quantum number $J = 1$. The possible deexcitation to the lower bound state $J = 0$ is closely connected with the probability of the fusion reaction in such a molecule. Theoretical estimations for the fusion rates for the reaction

$$d\mu^3\mathrm{He} \rightarrow \mu + {}^4\mathrm{He} + p + 18.35\ \mathrm{MeV} \quad (6)$$

in the state $J = 0$ surpass the estimated values of the fusion rates in the $J = 1$ state by orders of magnitude [11]. Therefore, the rate for the transition $J = 1 \rightarrow J = 0$ must be high in comparison to the rates of all the other decay channels of the muonic molecule to allow the observation of fusion events experimentally. For $(d\mu^4\mathrm{He})^*$ case, no measurable fusion is expected. Experimental investigations of the fusion process for $(d\mu^3\mathrm{He})^*$ are under way [12,13]. For theoretical and experimental investigations of this topic, an accurate knowledge of the molecular formation rates is essential. Moreover, the x-ray line shape reflects the populations of the two rotational states. Theoretical interest has focused on calculations of the probabilities of the three individual decay channels and the shape of the emitted x-ray spectrum in connection with the population of the rotational states [14–16], and with the correlated nuclear fusion rate in $(d\mu^3\mathrm{He})^*$ molecules [11,17–20].

### B. Experimental situation

Several previous experiments were stimulated by the proposal of a transfer process from hydrogen to helium via the formation of a metastable molecule [5]. The molecular exchange mechanism was confirmed by measuring high transfer rates of the expected order of magnitude. All the given transfer rates are normalized to liquid-hydrogen density and helium concentration. Therefore, they have to be multiplied by the target density $\phi$ and the atomic helium concentration $c_{\mathrm{He}}$ to obtain the ''effective transfer rates'' for a specific target composition.

Indirectly, transfer rates were obtained from the time distributions of $dd$ fusion events [21–25] or by the triple mixture method, which is to add a small component of a noble gas to the hydrogen-helium mixture to observe x-ray transitions of the muonic cascade in a noble gas [26,27]. Up till now the latter method was used only for a determination of the transfer rate from hydrogen to helium $\lambda_{p\mathrm{He}}$. In addition, molecular decay x rays were directly detected for the $(d\mu\mathrm{He})^*$ [28] case as well as the $(p\mu^4\mathrm{He})^*$ [29] case. Taking into account the particle decay process, the disagreement between yield [29] and triple-mixture measurements [26] of the transfer rates from hydrogen to $^4$He could be explained. Experimental results from mixtures of purified hydrogen ($^1H_2$) and helium were also presented by our collaboration. Results were obtained from triple-mixture measurements [30], as well as from investigations in binary mixtures [31]. In these measurements x rays originating from the decay of $(p\mu^3\mathrm{He})^*$ molecules were detected for the first time [31]. Measurements in deuterium-helium mixtures are additionally of interest because the molecular formation rates depend on the masses of the involved particles. Generally, transfer rates to helium are expected to be higher from muonic deuterium than from muonic hydrogen, and are therefore easier to measure directly in deuterium-helium mixtures. An isotopic effect between $^3$He and $^4$He is also expected. This isotopic effect was not seen in our investigations in hydrogen-helium mixtures [30,31]. In deuterium-helium mixtures this difference can be more precisely measured by direct x-ray measurements. The discrepancy between the results for the $D_2$-$^4$He case obtained by fusion event measurements [23,25] is still unexplained. In the first measurements of muon transfer rates via direct observation of the molecular x rays in deuterium-helium mixtures, which were carried out in liquid mixtures at KEK, Japan, a distinct line was observed in $D_2$-$^4$He mixtures, whereas the molecular line was very difficult to recognize in $D_2$-$^3$He mixtures [28,32]. The obtained results for the muon transfer rate to $^4$He could not be repro-

duced by the same group by measurements with different helium concentrations [33]. The result for $D_2$-$^4$He presented in Ref. [28] was corrected [32], giving rise to a remarkable difference between the result from those x-ray measurements and the fusion event measurements [23,25]. For the transfer rate from $(\mu d)_{1s}$ to $^3$He, only an upper limit was obtained [32].

### C. Advantages of this experiment

One advantage of the present experiment was the simultaneous employment of semiconductor diodes as x-ray detectors, and of electron counters, which allowed the application of an efficient reduction of background events. A continuous muon beam of high luminosity and high purity, at the Paul Scherrer Institut (PSI), Switzerland, was an additional benefit. Another important improvement in the present experiment was the use of a cryogenic gas target which allowed the selection of target conditions (concentrations and densities) in order to optimize the x-ray yield and the decay constant of the x-ray time distribution, which is also dependent on the experimental conditions. The helium concentrations for measurements in liquid targets are limited by the solubility of helium in liquid hydrogen.

## II. EXPERIMENT

### A. Goals

The goals of this work were to reach a significantly better yield for the decay x rays from the molecular $(d\mu\mathrm{He})^*$ state for both helium isotopes $^3$He and $^4$He, in comparison to earlier measurements [28,32,33], in order to investigate the energy and shape of the molecular x-ray spectrum, and to determine unambiguously the transfer rates from the time distributions of these x rays for both isotopic mixtures. The aim of these efforts was to improve the unsatisfactory experimental situation concerning the muon transfer rates, and to provide a possibility to test the different theoretical approaches.

### B. Setup

The measurements were carried out at the $\mu E4$ muon channel at PSI. The primary proton beam current was $\sim 1$ mA during the measurements. The muon beam was defined by a $1.7\times 1.7$ cm$^2$ opening area of the extraction slits. We performed three measurements each for the liquid and the gas states: one in a $D_2$-$^4$He mixture, one in a $D_2$-$^3$He mixture, and one in a pure deuterium target as background measurement.

A schematic view of the experimental setup used for the gas measurements is shown in Fig. 1. The cryogenic target cell was located in an insulation vacuum chamber. Two target cells were specially manufactured, one for the liquid mixture and one for the gas mixture. The liquid cell was constructed with a volume of 40 cm$^3$ for a temperature range of 20–25 K. It was made of stainless steel (type 1.4301), and coated by a 100 $\mu$m silver layer to avoid x-ray lines in the energy region of interest. The gas target cell for low temperatures had an inner volume of about 200 cm$^3$. The outer dimensions were $6.5\times 6.5\times 11$ cm$^3$ with an inner diameter

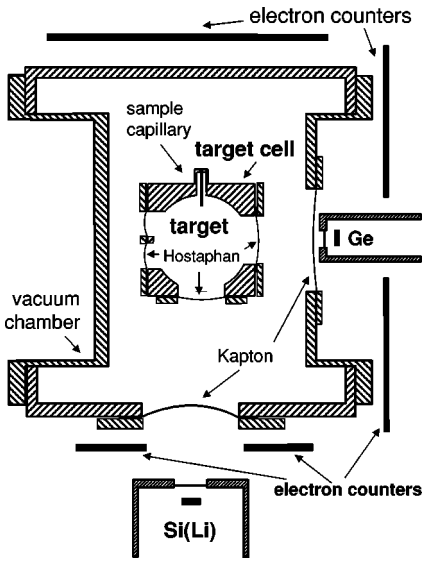


FIG. 1. Scheme of the experimental setup viewed along the muon beam. This setup was used for the measurements in gaseous mixtures. Two semiconductor diodes [Si(Li) and Ge] were employed. For measurements in liquid mixtures, a smaller target cell and only one diode were in use.

of 5.4 cm and an inner length of 7.75 cm. It consisted entirely of pure aluminum. Therefore, a silver coating was not needed. This target cell was also employed in our measurements in binary hydrogen-$^4$He mixtures [31].

A high target pressure is important for an optimum muon stopping distribution inside the target cell. On the other hand, the maximum possible target pressure depends on the total area and shape of the target windows, and the thickness and elasticity of the window material. Thick windows allow higher pressures, but thin windows are required for efficient transmission of low-energy x rays.

For the measurement in liquid mixtures, a 100-$\mu$m aluminum foil served as an entrance window for the muons. The window at the bottom of the liquid target cell was made of 25 $\mu$m Kapton, and the one on the detector side was made of 12.5 $\mu$m Kapton. The windows were laid out for a maximum pressure of 2 bar. In the gas target cell, the windows on the side and that on the bottom were made of 50-$\mu$m Hostaphan foils. A 75 $\mu$m Kapton foil served as entrance window for the muons. The windows of the gas target cell were designed for a pressure up to 7 bar, which at 30 K corresponds to a target density of $\sim$10% of the atomic liquid hydrogen density (LHD) (the LHD is equal to $4.25\times 10^{22}$ atoms cm$^{-3}$). The measured burst pressure was 20.2 bar. The windows on the vacuum chamber consisted of 50-$\mu$m Kapton foils on the side and on the bottom for both configurations, and the entrance window was made of 98 $\mu$m aluminum.

### C. Detectors

Two diodes were employed, one Si(Li) diode and one Ge diode, with 1- and 0.25-cm$^3$ sensitive volumes, respectively (see Fig. 1). Both energy and timing information of x rays were recorded. The target mixtures were also checked for

possible impurities with these detectors by searching for muonic x rays of higher $Z$ materials.

The energy resolution $\triangle E$ (full width at half maximum) at an energy of 6.4 keV (Fe $K\alpha$) was $\triangle E = 278$ eV for the Ge diode, and $\triangle E = 436$ eV for the Si(Li) diode in the environment of the accelerator. The sensitive energy region was 3–72 keV for the Ge diode and 5.5–152 keV for the Si(Li) diode.

The energy calibration of both detectors used for the gas mixtures was done with the help of x-ray lines originating from $^{54}$Mn, $^{55}$Fe, $^{57}$Co, and $^{241}$Am sources, and the muonic helium lines of known energy: $\mu^3$He K$\alpha$ (8.161 keV), $\mu^3$He K$\beta$ (9.668 keV), $\mu^4$He K$\alpha$ (8.235 keV), and $\mu^4$He K$\beta$ (9.755 keV). The stability of the energy calibration was carefully checked by determining the positions of the same lines every 3 h. Fluctuations occurred only within the statistical errors of the positions of each subsample.

Two plastic scintillators placed between the muon channel and the vacuum chamber served as a beam telescope. An anticoincidence between these detectors produced the muon stop signal which defined the time zero point. A pileup gate in the electronics was used to prevent a muon pileup for 8 $\mu$s before and after the muon stop. The scintillators arranged around the target cell, which are shown in Fig. 1, were used for the detection of the electrons from muon decay.

Additionally, CCD's and neutron counters were employed simultaneously with the semiconductor diodes. These dedectors are not indicated in the scheme of Fig. 1, since the analysis and the results of their measurements are beyond the scope of this work and will be discussed in a coming publication. Results obtained from the CCD detectors for the $(p\mu\mathrm{He})^*$ case are already published [31].

### D. Gas handling and mixture analysis

The target was cooled by a water-cooled helium compressor. The temperature was controlled by a proportional-differential-integral heating regulation system. The target cells were filled volumetrically. The gas mixtures were prepared close to the point of liquefaction as a compromise between the lowest possible pressure and high density.

An extraction capillary led directly into the target cell for sample taking. The gas-filling tube and the extraction capillary were fixed outside the target cell, with the opening in the center of the upper wall of the target cell. Several samples of the target fillings were taken before, during, and after each measurement to monitor the stability of the composition of the target mixtures. The target pressure and target temperature were monitored continuously during all measurements. After a measurement, the target was expanded into a storage volume which provided the possibility of analyzing the composition again any time after the measurement. The exact knowledge of the target composition is essential since the concentrations appear in nearly every rate which is used for the calculation of the final result of the measurement. Three to four samples were usually taken and analyzed at the same time. The results were compared with the volumetric determination of the concentrations during target filling and with the results of the analysis of the stored target mixture. The results of each analysis were consistent within their errors for all measurements.

Two systems were employed for the mass spectrometry, a quadrupole mass spectrometer (QMS) and a cyclotron resonance mass spectrometer (Omegatron). We used the QMS mainly for the analysis of the $D_2$-$^3$He mixtures because of its simpler handling, and the results were spot checked with the Omegatron. The Omegatron had to be employed for the investigation of mixtures with two ingredients of mass $\sim 4$, because it provides the high resolution required to separate the masses of $D_2$ and $^4$He.

A different procedure had to be carried out for the liquid targets as gaseous helium had to be dissolved in liquid deuterium. The composition of the target had to be determined volumetrically with the help of Henry's law proportionality constants [34].

The permeability of helium through polyamide foils (Kapton, Hostaphan) was systematically tested in our laboratory. The gas loss was found to be negligible below 125 K [35] for our type of measurements. Nevertheless, a second QMS was connected to the volume of the vacuum chamber to check that no helium diffuses out of the target cell during a measurement. Most parts of our gas handling and target system were also used for measurements in the hydrogen-helium mixtures [30,31].

### E. Target conditions

Our first three measurements were carried out in liquid targets because of the high muon stopping probability and the expected high photon yield, even at very low helium concentrations. In addition, measurements with liquid targets allow a direct comparison with the results obtained at KEK [28,32,33], and having obtained the preliminary results for the muon transfer rate we were able to optimize the target conditions for the gas measurements. Table I lists all of the target conditions. We used cleaned deuterium with a very low content of $^1H_2$ and HD molecules. In the calculation of the final result of the transfer rate for the liquid mixtures, the same concentration of HD as in the gas mixtures was taken into account. The selected muon momenta were $\sim 44.9$ MeV/$c$ for the measurements in liquid targets and $\sim 37.2$ MeV/$c$ for the gas measurements.

## III. ANALYSIS AND RESULTS

### A. Characteristics of the molecular x-ray line

We have clearly observed a $(d\mu\mathrm{He})^*$ decay spectrum with good statistics for both helium isotopes. These data allowed a precise investigation of the energy and shape of the molecular x-ray peak. Selection of different time windows after the muon stop showed that the molecular $(d\mu\mathrm{He})^*$ peak in the energy spectrum appeared only after the prompt x-ray lines (in coincidence with the muon stop signal), e.g., from a direct atomic capture of the muon in helium. The time distribution of the molecular peak showed a fast buildup ($<30$ ns) and then an exponentially decaying slope. For a comparison of the measured energy spectra with theory, a window was set at a time when all prompt x rays had disap-

TABLE I. Target conditions of all measurements. $T$ (K) indicates the temperature in Kelvin; $P$ (bar) the pressure in bar; the density is given relative to the liquid hydrogen density LHD; $C_{He}$ is the atomic helium ($^3$He or $^4$He) concentration; and $C_{HD}$ is the atomic concentration of HD molecules. Targets at a temperature of 23.8 K were liquid, the others gaseous.

| Target | $T$ (K) | $P$ (bar) | Density (LHD) | $C_{He}$ (%) | $C_{HD}$ (%) |
|---|---|---|---|---|---|
| $D_2$ | $23.8\pm0.1$ | $1.055\pm0.005$ | $1.145\pm0.006$ | | |
| $D_2$-$^4$He | $23.8\pm0.1$ | $1.055\pm0.005$ | $1.145\pm0.006$ | $0.140\pm0.014$ | |
| $D_2$-$^3$He | $23.8\pm0.1$ | $1.055\pm0.005$ | $1.145\pm0.006$ | $0.0880\pm0.0088$ | |
| $D_2$ | $31.5\pm0.2$ | $5.60\pm0.01$ | $0.0783\pm0.0007$ | | $0.3\pm0.1$ |
| $D_2$-$^4$He | $31.5\pm0.2$ | $5.51\pm0.01$ | $0.0792\pm0.0008$ | $3.25\pm0.05$ | $0.5\pm0.1$ |
| $D_2$-$^3$He | $30.5\pm0.2$ | $5.58\pm0.01$ | $0.0697\pm0.0007$ | $9.13\pm0.27$ | $0.4\pm0.1$ |

peared, in order to cut off the beam-correlated background. The shape of the background in the observed energy region and its time distribution were well known from the measurements in pure deuterium.

The intensity maximum of the molecular x-ray peak does not lie in its center; rather, the peak is asymmetric with a tail on the lower-energy side, and therefore it cannot be fitted by a single Gaussian. The peak is considerably broader than the energy resolutions of the detectors.

The energy maximum of the line moves to higher energies with the increasing mass of the helium isotope and for higher rotational quantum numbers. The accuracy of the obtained energy spectra made a comparison with theoretical spectra [15,16] possible. Using the theoretical energy spectra as input, we calculated experimental spectra by correcting for the efficiency of the x-ray detection and folding with the detector resolution for the Ge diode. The Ge diode was chosen because of its superior energy resolution. Figure 2(a) shows the calculated detection efficiency of the Ge detector. Details of the different contributions are found in Ref. [36]. The result of the procedure is shown in Fig. 2(b). In Fig. 3 the ''quasiexperimental'' spectra are compared with those actually measured. The positions of the intensity maxima of the molecular lines were determined for the theoretical and measured spectra in the same way, and are given in Table II. The widths of the measured spectra were determined to be

$$910\pm30 \text{ eV for the } (d\mu^3\text{He})^* \text{ line,}$$

$$910\pm20 \text{ eV for the } (d\mu^4\text{He})^* \text{ line.}$$

These values represent the weighted means of the measured spectra of both detectors. According to theory, a smaller width is expected for $(d\mu^4\text{He})^*$ than for $(d\mu^3\text{He})^*$. Figure 3 shows that the agreement between adapted theory spectra and measured ones is visibly better for $(d\mu^4\text{He})^*$ than for $(d\mu^3\text{He})^*$. Comparing the experimental and theoretical line shapes and the positions of the intensity maxima, we conclude that the radiative decay of the $(d\mu\text{He})^*$ molecule takes place primarily from the rotational state $J=1$ for both types of molecules, $(d\mu^3\text{He})^*$ and $(d\mu^4\text{He})^*$, for the investigated target conditions.

Theoretical works comparing their spectra with our experimental spectra, without taking into account the distor-

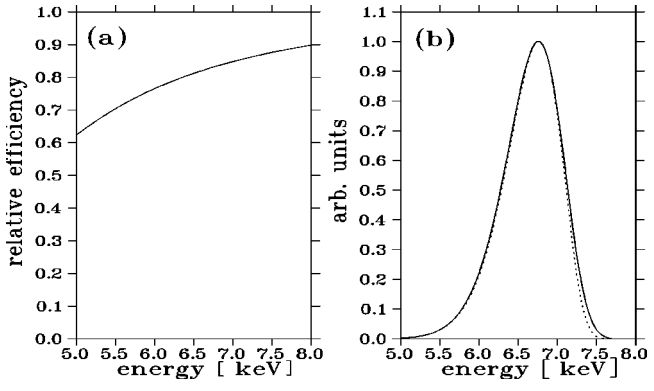


FIG. 2. (a) Relative x-ray detection efficiency of the Ge detector in the relevant energy region, taking into account the transmission through the target, the windows on the target cell and on the vacuum vessel, the beryllium window of the diode, and the absorption of the diode. (b) Theoretical energy spectrum (dotted line) [15], and the same spectrum but modified by taking into account the efficiency and energy resolution of the detector (solid line). Both spectra are normalized to the same height. The same procedure applied to the theoretical spectra from Ref. [16] lead to comparable results.

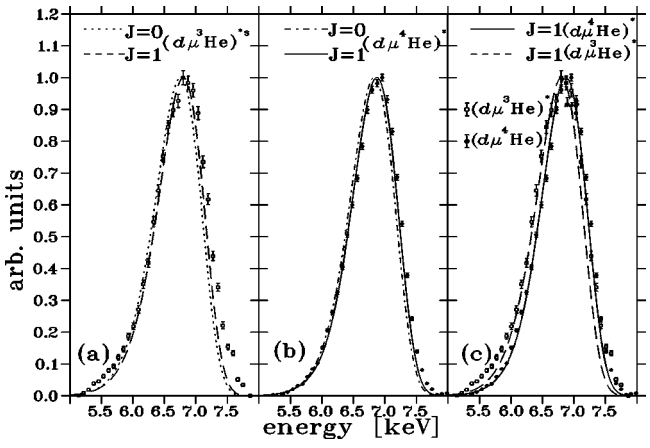


FIG. 3. Energy spectra for the molecular x-ray peak. The spectra from theory are adapted to our experimental conditions and compared with the measured spectra: (a) $(d\mu^3\text{He})^*$. (b) $(d\mu^4\text{He})^*$. (c) The two experimental spectra for both isotopic compositions together with the respective theoretical expectations for $J=1$. The theory spectra shown here are taken from Ref. [15].

TABLE II. Energy of the intensity maximum of the molecular decay spectrum in keV.

| | $(d\mu^3\mathrm{He})^*$ | | $(d\mu^4\mathrm{He})^*$ | |
|---|---|---|---|---|
| | $J=0$ | $J=1$ | $J=0$ | $J=1$ |
| This experiment | $6.80\pm0.03$ | | $6.88\pm0.03$ | |
| Theory [15] | 6.766 | 6.808 | 6.836 | 6.878 |
| Theory [16] | 6.760 | 6.782 | 6.836 | 6.857 |

tions due to detector efficiency and energy resolution, came to the same conclusion [15,16] because the change of the energy spectrum due to the experimental conditions was very small after normalization of the original theory spectrum and the adapted one to the same height [Fig. 2(b)]. The difference between the results of both calculations [15,16] is too small to allow any selection between them from the experimental data.

### B. Determination of the muon transfer rates

#### *1. Analysis method*

Figure 4 shows the most important reactions in a deuterium-helium mixture in which a muon has stopped. The muon can either be captured in an excited state by a helium atom with a probability $W_{\mathrm{He}}$ or by a deuterium atom with a probability $W_d$. The formation of such an exotic atom is possible mainly by the transfer of the binding energy to one electron of the atom (Auger mechanism). A captured muon cascades down to the ground state of the atom via a series of transitions [37]. For a muonic deuterium atom, the cascade processes compete with excited-state transfer to helium atoms of the rates $\lambda_{d\mathrm{He}^*}$. The probability for a muonic deuterium atom to reach its ground state in the presence of helium is called $q_{1s}^{\mathrm{He}}$. The muon transfer from a ground-state deuterium atom $(\mu d)_{1s}$ to a helium atom takes place predominantly via the formation of the metastable, excited $(d\mu\mathrm{He})^*$ molecule [5]; direct transfer is suppressed [4].

For a $(\mu d)_{1s}$ atom, there exist several other reaction channels which must be taken into account in our analysis: muon decay, transfer to possible target impurities or to atoms of the target cell walls (muon transfer rates to higher $Z$ elements are generally significantly larger than to helium), and formation of a $p\mu d$ molecule with another proton or, more likely, a $d\mu d$ molecule with a deuteron. The $d\mu d$ molecular formation rates $\lambda_{d\mu d}^{1/2}$ and $\lambda_{d\mu d}^{3/2}$ from the two hyperfine states $F=\frac{1}{2}$ and $\frac{3}{2}$, where $F$ is the total spin of the $(\mu d)_{1s}$ atom, show a significantly different temperature dependence due to the different level energies [38,39]. Spontaneous fusion of the two nuclei of the $d\mu d$ molecule follows.

In pure deuterium, there are two fusion channels:

$$d\mu d \rightarrow \mu + t + p, \tag{7}$$

$$d\mu d \rightarrow \mu + {}^3\mathrm{He} + n. \tag{8}$$

In the second channel, the muon may ''stick'' to the $^3$He nucleus being lost for further fusion reactions. The average sticking probability is $\omega = \beta\ \omega_d$, where $\beta$ is the probability

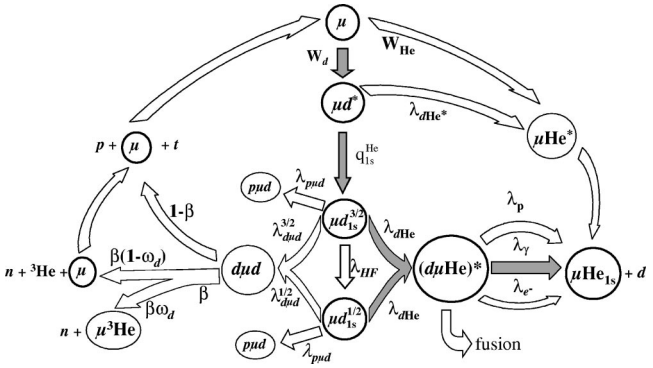


FIG. 4. Scheme of the most important kinetic processes in a deuterium-helium mixture when a muon is introduced. The muon may be captured either by a deuterium atom or a helium atom, and cascade down via various cascade processes to the ground state. The ground state of muonic deuterium $(\mu d)_{1s}$ which exists in the two hyperfine states $F=\frac{3}{2}$ and $F=\frac{1}{2}$, is reached with the probability $q_{1s}^{\mathrm{He}}$. A $p\mu d$ or $d\mu d$ molecule may be formed, the latter leading to muon-catalyzed fusion. The muon transfer process from $(\mu d)_{1s}$ to helium proceeds with high probability via the formation of a $(d\mu\mathrm{He})^*$ molecule which has four disappearance channels. The steps of the muon transfer process are drawn bold. For a more detailed explanation of the kinetics, see the text (Sec. III B 1).

for a $dd$ fusion channel with a neutron and a helium nucleus as the end products [Eq. (8)], and $\omega_d$ is the sticking probability of the muon to the helium nucleus after fusion.

The formation of a $(d\mu\mathrm{He})^*$ molecule is possible from both hyperfine states of a $(\mu d)_{1s}$ atom. The hyperfine transition rate in $(\mu d)_{1s}$ atoms is much higher than the muon decay rate. The populations of the two hyperfine states of the $(\mu d)_{1s}$ atom ($N_{1/2}$ and $N_{3/2}$) and the population of the $(d\mu\mathrm{He})^*$ molecular state ($N_{d\mu\mathrm{He}}$) are described by a system of differential equations with constant coefficients. At the low temperatures of this experiment, the upward hyperfine transition $F=\frac{1}{2}\rightarrow F=\frac{3}{2}$ is negligible. Neglecting this transition and the muon recycling after fusion, the time evolution of states is described by the following linear differential system:

$$\frac{dN_{3/2}}{dt} = -[\lambda_0 + \varphi(C_d\lambda_{d\mu d}^{3/2} + C_d\lambda_{HF} + C_{\mathrm{He}}\lambda_{d\mathrm{He}})]N_{3/2}, \tag{9}$$

$$\frac{dN_{1/2}}{dt} = +\varphi C_d\lambda_{HF}N_{3/2} - [\lambda_0 + \varphi(C_d\lambda_{d\mu d}^{1/2} + C_{\mathrm{He}}\lambda_{d\mathrm{He}})]N_{1/2}. \tag{10}$$

Here $\lambda_0$ is the muon decay rate, $\lambda_{HF}$ is the hyperfine transition rate $F=\frac{3}{2}\rightarrow F=\frac{1}{2}$, $C_d$ and $C_{\mathrm{He}}$ are the atomic deuterium and helium concentrations, respectively, and $\varphi$ is the target density relative to the LHD.

We assume the muon transfer rate to helium $\lambda_{d\mathrm{He}}$ to be equal from both hyperfine states, an assumption supported by theory [40]. Then the population of the $(d\mu\mathrm{He})^*$ state can be written as

$$\frac{dN_{d\mu\mathrm{He}}}{dt} = \varphi C_{\mathrm{He}} \lambda_{d\mathrm{He}} (N_{1/2} + N_{3/2}) e^{-t\lambda_{exp}}. \qquad (11)$$

Since the decay rate of the muonic molecule ($\lambda_{dec} \sim 10^{12}$ s$^{-1}$) is much higher than the molecular formation rate, the muon transfer rate is determined mainly by the $(d\mu\mathrm{He})^*$ formation rate [5]. The measured time distribution of the $(d\mu\mathrm{He})^*$ x-ray peak is very well described by a single exponential with the rate $\lambda_{exp}$, which is interpreted as the total disappearance rate of the $(\mu d)_{1s}$ state in a $D_2$-He mixture.

In this approximation, $\lambda_{exp}$ is given by

$$\lambda_{exp} = \lambda_0 + \varphi \left( C_d \omega \lambda_{d\mu d}^{1/2} + C_{\mathrm{He}} \lambda_{d\mathrm{He}} + C_p \lambda_{p\mu d} + \sum_i C_i \lambda_i \right), \qquad (12)$$

where $C_p$ is the atomic concentration of hydrogen $^1$H, $\lambda_{p\mu d}$ is the formation rate of the $p\mu d$ molecule, and $C_i$ are the concentrations of possible target impurities with the corresponding muon transfer rates $\lambda_i$. With $\omega$, we have reintroduced the average sticking probability.

Numerical tests showed that the approximate form Eq. (12) reproduces the calculated exact solution of the linear differential equation system very accurately. The relative systematic uncertainty due to the use of this approximate equation for our analysis is $<10^{-4}$ [36], and therefore negligible in comparison with the statistical errors of our results.

#### *2. Event types*

Five event types can be detected by our x-ray detectors.

(1) X rays of about 6.8 keV originating from the decay of the $(d\mu\mathrm{He})^*$ molecule.

(2) X rays from the muonic cascade in helium. The energy of the x rays from the muonic cascade in deuterium are below the sensitive regions of the diodes.

(3) X rays from the cascade of muons captured by atoms of the target cell or detector materials.

(4) Delayed x rays from the muonic cascade in atoms of the target cell material, which are due to diffusion of $\mu d$ atoms within the target. When they reach the target cell wall, muon transfer is possible.

(5) Muonic x rays from the cascade in impurity atoms with $Z \geqslant 3$, which may be present in the deuterium-helium mixture.

(6) A continuous background, e.g., from bremsstrahlung.

Prompt events of types (2), (3), and (5) do not influence the time distribution of the 6.8-keV x rays, whereas delayed events of types (4) and (5) would cause additional delayed components which must be taken into consideration in the evaluation of the muon transfer rate. We identified prompt muonic aluminum and muonic oxygen lines during the measurements in the gas targets. Oxygen is present in the window foils of the target cell, while aluminum can be assigned to the target cell walls. The investigation of all visible lines showed that all lines except the 6.8-keV line, and the muonic helium lines had no delayed components.

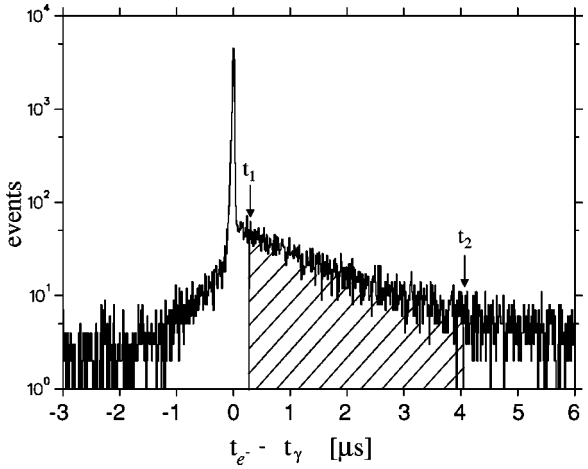


FIG. 5. Time difference spectrum of the first signal from any electron counter and of the Si(Li) diode after the muon stop. The hatched region shows the allowed time interval $(t_1, t_2)$ for the electrons to follow the x-ray event (in this case 310 and 4010 ns after the muon stop] for the creation of the final time spectrum.

We did not find gas impurities by our mass spectrometer measurements. One would primarily expect a contamination by nitrogen, of which only a few ppm would be clearly visible in the energy spectra. We did not observe any nitrogen line within our detection range (e.g., the $L$ lines at 19.033 keV, 25.683 keV, 28.761 keV etc.). Additionally, at cryogenic temperatures it is safe to assume that all conceivable target impurities are frozen out at the target walls, the target mixture itself is clean.

The muonic helium lines were different from all of the other peaks. Their time distributions showed delayed events caused by muons, which either ''stick'' to the helium nucleus or are recycled and captured by helium atoms after catalyzing $dd$ fusion. Simulations for our measurements showed that, e.g., for the gaseous $D_2$-$^3$He mixture $\simeq 0.1\%$ of the total amount of $\mu$He events are expected to be delayed $K\alpha$ x rays. This is consistent with the observed spectrum. The time constant of these delayed events is different from that of the $(d\mu\mathrm{He})^*$ line. Moreover, in our measurements with hydrogen-helium targets [31], no delayed part of the $\mu$He line was discovered.

#### *3. Evaluation of the muon transfer rates*

Two methods of background treatment were applied independently. One very efficient method makes use of the so-called ''delayed electron condition.'' This requires the detection of an electron from muon decay within a certain time interval after the x-ray signal. Using this method, x rays mainly from bremsstrahlung and from muon stops in target materials create a smooth background which can be efficiently suppressed. The time window for the detection of the delayed electron is selected with the help of a time difference spectrum of diode time signals and electron counters time signals (Fig. 5). However, the small detection efficiency of the electron counters due to their restricted solid angle leads to essential losses of good events. The application of the

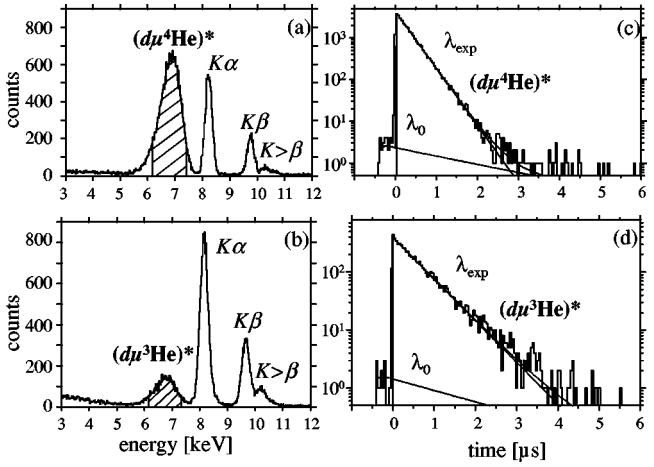


FIG. 6. Energy spectra of the muonic decay x rays from (a) $(d\mu^4\mathrm{He})^*$ and from (b) $(d\mu^3\mathrm{He})^*$ obtained in the gaseous mixtures. $K\alpha$ and $K\beta$, $K>\beta$, indicate the respective muonic helium x-ray lines originating from the muonic cascade in (a) $^4$He or (b) $^3$He. (c) and (d) show the respective time distributions corresponding to the hatched regions in (a) and (b). For the background suppression, a delayed electron condition was applied. $\lambda_0$ is the slope of the accidental background.

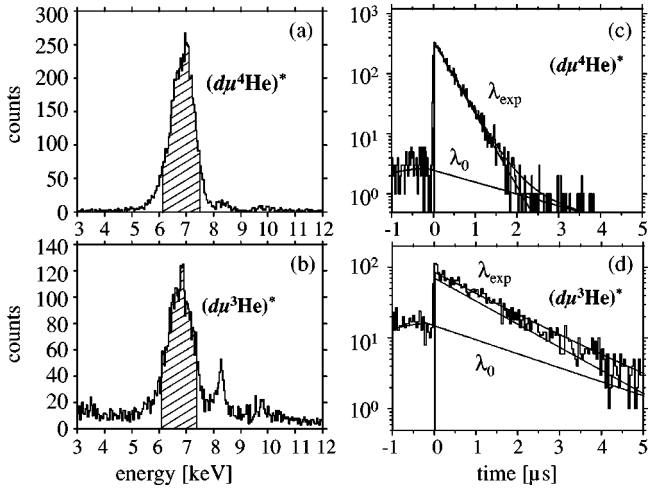


FIG. 7. The energy spectra of the muonic decay x rays from $(d\mu^4\mathrm{He})^*$ (a) and $(d\mu^3\mathrm{He}^*)$ (b), obtained in the liquid mixtures are shown. For the displayed time distributions in (c) and (d) only events in the energy range of the hatched regions in (a) and (b) were accepted. For background suppression, a delayed electron condition was applied, $\lambda_0$ is the slope of the accidental background due to the application of this condition.

delayed electron condition changes the constant accidental background to a well-known exponential shape [41,42].

After the background shape is determined, the time distribution of the x-ray events from the decay of the muonic molecules can be fitted by a single exponential. The fit range was chosen to fulfill two conditions: more than 30 events per channel, and more than 20 degrees of freedom. The stability of the result with respect to variable fit ranges was carefully checked. Influences of the time resolution functions of the detectors were studied and found to be negligible [36]. Figures 6 and 7 show the observed energy spectra and the respective time distributions. Table III gives the fit results for $\lambda_{exp}$. The measurements in the gas mixtures with two different, simultaneously operating, detectors represent independent measurements at the same experimental conditions. Since the results are consistent with each other, the weighted mean was formed. For the measurements in liquid targets, only the Si(Li) diode was employed.

The second method of background treatment applied was simple subtraction of the background beneath the 6.8-keV line. The shape of the background was extracted from the measurements in pure deuterium. This known background was subtracted from the spectrum obtained in the mixtures using the correct normalization. For the determination of the statistical relation of both spectra, the energy regions between 15 and 70 keV were compared because there are no structures correlated to the helium admixture. The time calibrations of both diodes were stable within $\pm 1$ ns, so that no corrections had to be carried out before the subtraction of the time spectra. The time spectra obtained by background subtraction could be fitted by a single exponential.

Both methods of background treatment were applied to the data of each detector for each of the measurements. The results of both methods and of each detector were consistent with each other. Since the spectra obtained by applying a delayed electron condition allowed a more precise analysis, the fit results for $\lambda_{exp}$ obtained from these spectra (Table III) were used to calculate the muon transfer rate $\lambda_{d\mathrm{He}}$ with Eq. (12). The other necessary values were taken from the literature: the muon decay rate $\lambda_0 = (0.4551599 \pm 0.0000083)$

TABLE III. Fit results for the slope of the x-ray time spectra of the deexcitation $(d\mu\mathrm{He})^*$ line which were obtained by applying a delayed electron condition. $\chi^2_{red}$ is the $\chi^2$ per degree of freedom of the fit curve.

| Target | Detector | Fit range ($\mu$s) | $\lambda_{exp}(\mu s^{-1})$ | $\chi^2_{red}$ |
|---|---|---|---|---|
| $D_2$-$^3$He gaseous | Ge | (0.5, 1.65) | $1.595 \pm 0.072$ | 0.954 |
| | Si(Li) | (0.06, 1.65) | $1.648 \pm 0.036$ | 0.771 |
| | weighted mean | | $1.637 \pm 0.032$ | |
| $D_2$-$^4$He gaseous | Ge | (0.13, 1.48) | $3.167 \pm 0.026$ | 0.935 |
| | Si(Li) | (0.12, 1.59) | $3.153 \pm 0.024$ | 1.25 |
| | weighted mean | | $3.159 \pm 0.018$ | |
| $D_2$-$^3$He liquid | Si(Li) | (0.11, 1.65) | $0.751 \pm 0.067$ | 1.01 |
| $D_2 - ^4$He liquid | Si(Li) | (0.1, 1.75) | $2.746 \pm 0.027$ | 0.896 |

TABLE IV. Experimental results for the ground state muon transfer rates from $(\mu d)_{1s}$ to $^3$He and to $^4$He. RT indicates room temperature, *dd* fusion events indicates that the results were obtained from detected events caused by *dd* fusion, and x rays stands for the measurement of molecular x rays. All results given were obtained from time distributions.

| Detected signals | $T$ (K) | $\lambda_{d^3\mathrm{He}}$ ($10^8$ s$^{-1}$) | $\lambda_{d^4\mathrm{He}}$ ($10^8$ s$^{-1}$) | Reference |
|---|---|---|---|---|
| x rays | $30.5\pm0.2$ | $1.856\pm0.077$ | | this work |
| | $31.5\pm0.2$ | | $10.50\pm0.21$ | this work |
| x rays | $23.8\pm0.1$ | $2.77\pm0.73$ | $14.2\pm1.4$ | this work |
| x rays | 20 | | $13.1\pm1.2$ | [28] |
| correction to Ref. [28] | | | 26.2 | [32] |
| x rays | 20–22 | $\leqslant 9$ | $28.1\pm1.2\pm4.0$ | [32] |
| *dd* fusion events | RT | | $3.2\pm0.3$ | [22] |
| *dd* fusion events | RT | $1.27\pm0.11$ | $3.68\pm0.18$ | [23] |
| *dd* fusion events | RT | $1.24\pm0.05$ | | [24] |
| *dd* fusion events | 300 | | $2.75\pm0.22$ | [25] |
| *dd* fusion events | 100–540 | $2\pm1$ | | [21] |

$\times 10^6$ s$^{-1}$ [43], the $d\mu d$ molecular formation rate $\lambda_{d\mu d}^{1/2} = (0.0468\pm0.0054)\times10^6$ s$^{-1}$ at 25.5 K, and the branching ratio for the fusion channel with neutron release $\beta = 0.530 \pm 0.021$ at 25.5 and 40 K [44], the $p\mu d$ molecular formation rate $\lambda_{p\mu d} = (5.6\pm0.2)\times10^6$ s$^{-1}$ at 20–23 K [45], and the sticking probability $\omega_d = 0.122\pm0.003$ [46].

Our results for $\lambda_{d\mathrm{He}}$ are summarized together with results of earlier measurements in Table IV. The transfer rate $\lambda_{d\mathrm{He}}$ obtained from $\lambda_{exp}$ represents the total ground-state muon transfer rate, which is the sum of the molecular transfer rate and the low direct ground-state transfer rate $\lambda_{d^{3,4}\mathrm{He}}^{dir} \sim 10^6$ s$^{-1}$ [4]. The different error contributions are specified in Table V. The errors of the values taken from the literature have very little influence on the uncertainties of our results.

A clear difference between the muon transfer rates in liquid and gas mixtures appears for both rates $\lambda_{d^4\mathrm{He}}$ and $\lambda_{d^3\mathrm{He}}$, which is significantly larger than expected due to the very small temperature difference [47]. Contrary to the gas mixtures, there could occur unknown systematic uncertainties of the helium concentrations in the liquid mixtures because of the determination method. However, these systematic errors, if relevant at all, could only slightly decrease the helium concentrations.

Regarding Eq. (12), possible lower helium concentrations than the ones given in Table I for the liquid mixtures only lead to higher transfer rates which would make the difference between the transfer rates measured in gas and liquid targets even more striking. Therefore, the difference between the rates can be assigned to the different densities of the mixtures. A possible explanation can be based on the different kinetic-energy distributions of $(\mu d)_{1s}$ atoms at different densities due to cascade processes. In particular, Coulomb deex-

TABLE V. Contributions of the individual errors of the quantities which are necessary for the evaluation of the transfer rate $\lambda_{d\mathrm{He}}$ to the total error. $\varphi$ indicates the target density, $C_{\mathrm{He}}$ the atomic helium concentration ($^3$He or $^4$He), and $C_p$ the atomic hydrogen concentration. $V_{lit}$ contains the values taken from literature: $\lambda_0, \lambda_{d\mu d}^{1/2}, \lambda_{p\mu d}, \beta,$ and $\omega_d$. rms means ''root mean square.'' All uncertainties are given in %.

| | Source of error | | | | | |
|---|---|---|---|---|---|---|
| | Fit | $\varphi$ | $C_{\mathrm{He}}$ | $C_p$ | $V_{lit}$ | rms |
| $D_2$-$^3$He gaseous | | | | | | |
| Uncertainty of source | 1.95 | 1.0 | 2.96 | 25.0 | 0.002–11.54 | |
| Resulting uncertainty for $\lambda_{d\mathrm{He}}$ | 2.71 | 1.0 | 2.96 | 0.02 | 0.003 | 4.1 |
| $D_2$-$^4$He gaseous | | | | | | |
| Uncertainty of source | 0.57 | 1.01 | 1.54 | 20.0 | 0.002–11.54 | |
| Resulting uncertainty for $\lambda_{d\mathrm{He}}$ | 0.67 | 1.01 | 1.54 | 0.008 | 0.002 | 2.0 |
| $D_2$-$^3$He liquid | | | | | | |
| Uncertainty of source | 9.0 | 0.52 | 10.01 | | 0.002–11.54 | |
| Resulting uncertainty for $\lambda_{d\mathrm{He}}$ | 24.16 | 0.55 | 10.06 | | 0.22 | 26 |
| $D_2$-$^4$He liquid | | | | | | |
| Uncertainty of source | 0.98 | 0.52 | 10.0 | | 0.002–11.54 | |
| Resulting uncertainty for $\lambda_{d\mathrm{He}}$ | 1.17 | 0.53 | 10.0 | | 0.03 | 10 |

citation leads to accelerated $(\mu d)_{1s}$ atoms [48]. Since thermalization of these atoms takes place essentially via elastic collisions, a larger high-energy fraction of $(\mu d)_{1s}$ atoms is present in the gas mixtures. As it is expected that the $(d\mu\mathrm{He})^*$ formation rate decreases with rising collision energies [5,7,8,47], the larger fraction of nonthermalized $(\mu d)_{1s}$ atoms in the gas mixtures leads to the observation of lower muon transfer rates than that corresponding to the actual temperature of the mixture. A confirmation of this explanation can only be reached by a full cascade calculation which also takes into account excited-state transfer processes. Such calculations are presently not available.

## IV. SUMMARY

We performed measurements in liquid and gaseous mixtures of $D_2$-$^3$He and $D_2$-$^4$He. The molecular x rays originating from the decay of the $(d\mu\mathrm{He})^*$ molecules were observed unambiguously. The measured width of the molecular x-ray peak is $910\pm30$ eV for $(d\mu^3\mathrm{He})^*$ and $910\pm20$ eV for $(d\mu^4\mathrm{He})^*$, both of which are greater than expected by theory. Comparing the experimental and calculated energy maxima of the peaks (Table II and Fig. 3), we found that the $(d\mu\mathrm{He})^*$ molecule primarily decays from the rotational state $J=1$ for our experimental conditions of the gas measurements (Table I).

The obtained muon transfer rates from $(\mu d)_{1s}$ to $^{3,4}$He are

$$\lambda_{d^4\mathrm{He}}=(14.2\pm1.4)\times10^8\mathrm{s}^{-1},$$

$$\lambda_{d^3\mathrm{He}}=(2.77\pm0.73)\times10^8\mathrm{s}^{-1}$$

in liquid targets at $23.8\pm0.1$ K, and

$$\lambda_{d^4\mathrm{He}}=(10.50\pm0.21)\times10^8\mathrm{s}^{-1},$$

$$\lambda_{d^3\mathrm{He}}=(1.856\pm0.077)\times10^8\mathrm{s}^{-1}$$

in gas targets at $\sim31$ K.

These results are compared with other available experimental results for the muon-transfer rates in Table V. Most experimentally determined transfer rates were obtained by the investigation of events following muon-catalyzed $dd$ fusion. However, the measurements were carried out at significantly different temperatures from ours; therefore, a direct comparison is not possible.

Our result of $\lambda_{d^4\mathrm{He}}$ obtained in liquid mixtures agrees well with the first reported results of x-ray measurements by the KEK group [28], but not with their correction of that value nor with their final value [32]. All the cited KEK values in Table V were obtained from time distributions of the molecular decay x rays. The theoretical estimations range from 1.76 to $3.12\times10^8$ s$^{-1}$ for $\lambda_{d^3\mathrm{He}}$, and from 3.34 to 11.8 $\times10^8$ s$^{-1}$ for $\lambda_{d^4\mathrm{He}}$ [7,8] for 0.004 eV. We cannot confirm the large discrepancy between theory and experiment at low temperature, but we also have not found a theoretical approach which consistently describes all our experimental results. The present result obtained from the gaseous $D_2$-$^4$He mixture is the most accurate one of all measurements reported up to now. Only an upper limit was given for $\lambda_{d^3\mathrm{He}}$ from decay x-ray measurements [32] until the present work. To our knowledge, our results for $D_2$-$^3$He are the first results obtained by direct x-ray measurement for this isotopic composition. The result for $\lambda_{d^3\mathrm{He}}$ obtained from the measurement with the gas target was recently confirmed by the preliminary result of another x-ray measurement at 32 K [12].

The expected isotopic difference between the transfer rate from deuterium to $^3$He or to $^4$He is unambiguously confirmed. The muon transfer rates from deuterium to helium are about one order of magnitude higher than those from hydrogen to helium. This huge difference is qualitatively in agreement with all theoretical expectations that the muon transfer rate scales with the reduced mass of the involved particles.

The observed difference between the results from the gas and liquid measurements is probably not only due to the rather small temperature difference, but can also be assigned to the different densities of the mixtures. A possible explanation is the different kinetic-energy distribution of $(\mu d)_{1s}$ atoms at different densities.

A set of values for the muon transfer rates from deuterium to helium is available for comparison with different theoretical approaches and calculations now. The experimental results reported here have already stimulated further theoretical work [19,47].

## ACKNOWLEDGMENTS

The authors are grateful to E. A. Kolganova and W. Czaplinski for providing calculated energy spectra of the $(d\mu\mathrm{He})^*$ x-ray emission. Financial support by the Austrian Academy of Sciences, the Austrian Science Foundation, the Swiss Academy of Sciences, the Swiss National Science Foundation, and the Beschleunigerlaboratorium der Universität und Technischen Universität München is gratefully acknowledged.

[1] W. H. Breunlich, P. Kammel, J. S. Cohen, and M. Leon, Annu. Rev. Nucl. Part. Sci. **39**, 311 (1989).

[2] S. B. Baziladze, P. F. Ermolov, and K. O. Oganesyan, Zh. Éksp. Teor. Fiz. **49**, 1042 (1965) [Sov. Phys. JETP **22/4**, 725 (1966)]; A. Alberigi Quaranta *et al.*, Nuovo Cimento **47/1**, 236 (1967); H. Daniel *et al.*, Nucl. Phys. A **345**, 409 (1980); L. Schellenberg, Muon Catal. Fusion **5/6**, 73 (1990/91), and references therein.

[3] D. R. Bates, F. R. S. Carson, and T. R. Carson, Proc. R. Soc. London, Ser. A **234**, 207 (1956).

[4] S. S. Gershtein, Zh. Éksp. Teor. Fiz. **43**, 706 (1962) [Sov. Phys. JETP **16/2**, 501 (1963)].

[5] Yu. A. Aristov *et al.*, Yad. Fiz. **33**, 1066 (1981) [Sov. J. Nucl. Phys. **33/4**, 564 (1981)].

[6] A. V. Kravtsov *et al.*, Phys. Lett. **83A**, 379 (1981).

[7] V. K. Ivanov *et al.*, Zh. Éksp. Teor. Fiz. **91**, 358 (1986) [Sov.

Phys. JETP **64**, 210 (1986)].
[8] A. V. Kravtsov, A. I. Mikhailov, and N. P. Popov, J. Phys. B **19**, 1323 (1986); **19**, 2579 (1986).
[9] S. Hara and T. Ishihara, Phys. Rev. A **39**, 5633 (1989).
[10] Y. Kino and M. Kamimura, Hyperfine Interact. **82**, 195 (1993).
[11] L. N. Bogdanova, S. S. Gershtein, and L. I. Ponomarev, Pis'ma Zh. Éksp. Teor. Fiz. **67**, 89 (1998) [JETP Lett. **67**, 99 (1998)].
[12] A. Del Rosso *et al.*, Hyperfine Interact. **118**, 177 (1999).
[13] E. M. Maev *et al.*, Hyperfine Interact. **118**, 171 (1999).
[14] A. V. Kravtsov, A. I. Mikhailov, and V. I. Savichev, Z. Phys. D: At., Mol. Clusters **29**, 49 (1994).
[15] V. B. Belyaev, O. I. Kartavtsev, V. I. Kochkin, and E. A. Kolganova, Z. Phys. D: At., Mol. Clusters **41**, 239 (1997).
[16] W. Czaplinski, A. Kravtsov, A. Mikhailov, and N. Popov, Phys. Lett. A **A233**, 405 (1997).
[17] M. Kamimura and Y. Kino, Nucl. Instrum. Methods Phys. Res. A **402**, 397 (1998).
[18] W. Czaplinski, A. Kravtsov, A. Mikhailov, and N. Popov, Eur. Phys. J. D **3**, 223 (1998).
[19] M. P. Faifman and L. I. Men'shikov, Hyperfine Interact. **118**, 187 (1999).
[20] L. N. Bogdanova, V. I. Korobov, and L. I. Ponomarev, Hyperfine Interact. **118**, 183 (1999).
[21] S. E. Jones *et al.*, Phys. Rev. Lett. **51**, 1757 (1983).
[22] D. V. Balin *et al.*, Phys. Lett. **141B**, 173 (1984).
[23] D. V. Balin *et al.*, Pis'ma Zh. Éksp. Teor. Fiz. **42**, 236 (1985) [JETP Lett. **42**, 293 (1985)].
[24] D. V. Balin *et al.*, in *Muonic Atoms and Molecules*, edited by L. A. Schaller and C. Petitjean (Birkhäuser, Basel, 1993), p. 25.
[25] V. M. Bystritskii *et al.*, Zh. Éksp. Teor. Fiz. **98**, 1514 (1990) [Sov. Phys. JETP **71**, 846 (1990)].
[26] R. Jacot-Guillarmod *et al.*, Phys. Rev. A **38**, 6151 (1988); **55**, 3447 (1997).
[27] S. Tresch *et al.*, Eur. Phys. J. D **2**, 93 (1998).
[28] T. Matsuzaki *et al.*, Muon Catal. Fusion **2**, 217 (1988).
[29] H. P. von Arb *et al.*, Muon Catal. Fusion **4**, 61 (1989).
[30] S. Tresch *et al.*, Phys. Rev. A **57**, 2496 (1998).
[31] S. Tresch *et al.*, Phys. Rev. A **58**, 3528 (1998).
[32] K. Ishida *et al.*, Hyperfine Interact. **82**, 111 (1993).
[33] Y. Watanabe *et al.*, Muon Catal. Fusion **5/6**, 93 (1990/91).
[34] M. J. Hiza, Fluid Phase Equilibria **6**, 203 (1981); P. C. Souers, *Hydrogen Properties for Fusion Energy* (University of California Press, Berkeley, 1986), pp. 187–191.
[35] B. Rinnhofer, Diploma thesis, University of Vienna, 1997 (unpublished).
[36] B. Gartner, Ph.D. thesis, University of Vienna, 1998 (unpublished).
[37] B. Lauss *et al.*, Phys. Rev. A **60**, 209 (1999).
[38] P. Kammel *et al.*, Phys. Rev. A **28**, 2611 (1983).
[39] A. Scrinci *et al.*, Phys. Rev. A **47**, 4691 (1993).
[40] M. P. Faifman (private communication).
[41] P. Kammel, Ph.D. thesis, University of Vienna, 1981 (unpublished).
[42] N. Nägele *et al.*, Nucl. Phys. A **493**, 397 (1989).
[43] P. D. Group, Eur. Phys. J. C. **3**, 280 (1998).
[44] J. Zmeskal *et al.*, Phys. Rev. A **42**, 1165 (1990).
[45] C. Petitjean *et al.*, Muon Catal. Fusion **5/6**, 199 (1990/91).
[46] D. V. Balin *et al.*, Pis'ma Zh. Éksp. Teor. Fiz. **40**, 318 (1984) [JETP Lett. **40**, 1112 (1984)].
[47] A. V. Kravtsov and A. I. Mikhailov (unpublished).
[48] V. E. Markushin, Phys. Rev. A **50**, 1137 (1994).